Electronic Supplementary Information

Insight on the Charge Transportation in Cadmium Based Semiconducting Organic-Inorganic Hybrid Materials and Their Application in the Fabrication of Photosensitive Schottky Devices

Sourav Roy[a,b⊥], Arka Dey[c,d⊥], Rosa M. Gomila,[e] Joaquin Ortega-Castro,[e] Antonio Frontera[e]*, Partha Pratim Ray,[c]*and Shouvik Chattopadhyay[a]*

*[a]Department of Chemistry, Inorganic Section, Jadavpur University, Kolkata - 700032, India.
Tel: +9133-2457-2941; E-mail: shouvik.chem@gmail.com*

[b]Solid State and Structural Chemistry Unit, Indian Institute of Science, Bangalore 560 012, India

[c]Department of Physics, Jadavpur University, Kolkata-700012, India. E-mail: partha@phys.jdvu.ac.in; Fax: +91 3324138917

[d] Department of Physics, National Institute of Technology Durgapur, Durgapur-713209, India

[e]Departament de Química, Universitat de les Illes Balears, Crta de Vall demossa km 7,5, 07122 Palma de Mallorca (Baleares), SPAIN, E-mail: toni.frontera@uib.es

X-ray crystallography

Suitable single crystals of both complexes were picked out and were mounted on a glass fibre. A 'Bruker D8 QUEST area detector' diffractometer equipped with graphite-monochromated Mo K$_\alpha$ radiation (λ = 0.71073 Å) has been used for X-ray data collection for complex **1**. Data integration and reduction were performed with the help of SAINT software and empirical absorption corrections were applied with SADABS programme.[1] A Rigaku Mercury 375/M CCD (XtaLAB mini) diffractometer using graphite monochromator Mo-Kα radiation were used for X-ray data collection for complex **2** and were processed with Rigaku crystal clear software (Rigaku, 2009). The structures were solved by SHELXT-2018 (Sheldrick,

2008) using direct methods embedded in the WinGX suite (Farrugia, 2012) of programs.[2,3] Full matrix least-squares refinements were carried out on F^2 for all non-hydrogen atoms using SHELXL-2017 (Sheldrick, 2015) with anisotropic displacement parameters.[4] The hydrogen atoms were added for all the atoms either from difference Fourier maps or in their calculated positions using the riding model. Mercury version 4.1.3 (Macrae et al., 2008) was used for molecular representations.[5]

Device fabrication

In this study, multiple metal-semiconductor (MS) junction devices were fabricated in ITO/synthesized complex/Al sandwich structure to perform the electrical study. In this regard, well dispersion of the synthesized complex was made in N,N-dimethyl formamide (DMF) by mixing and sonicated the right proportion (25 mg/ml) of the complex in separate vials. This newly prepared stable dispersion of the complex was deposited on the top of the ITO coated glass substrate by spun firstly at 600 rpm for 5 min and thereafter at 900 rpm for another 5 min with the help of SCU 2700 spin coating unit. Afterward, the as-deposited thin films were dried in a vacuum oven at 80 °C for several minutes to evaporate the solvent part fully. Here we used aluminium, deposited on a plain glass slide in the Vacuum Coating Unit as metal electrode by maintaining the effective area as 7.065×10^{-2} cm^{-2} with shadow mask. Using Sourcemeter made by Keithley (model no: 2635B), the current-voltage (I-V) characteristics of the devices was measured to analyse the electrical properties. All the device fabrication and measurements were carried out at room temperature and under ambient conditions.

Solid State Calculations

The geometries of complexes **1** and **2** were optimized with the DFT method using the CASTEP program code of Accelrys, Inc.[6] The atomic positions within the crystal were optimized while preserving the experimental unit cell parameters. For the calculations we used the GGA approximation; PBE functional[7,8] and ultrasoft pseudopotentials[9] with the relativistic treatment of the Koelling-Harmon[10]. A plane-wave basis set (300 eV cutoff) in the Γ points over the Brillouin zone were used. The energy tolerance for self-consistent field (SCF) convergence was $2\times10\text{-}6$ eV/atom for all calculations. The DFT-D dispersion correction has been included in the calculations with the Grimme scheme.[11] Band structures were calculated along the k-vector of the first Brillouin zone of the crystals, and Total and Partial density of states (TDOS and PDOS, respectively) of complexes **1** and **2** were plotted concerning the Fermi level with a 2x1x2 and 2x2x2 grids, respectively. The optical properties including dielectric function and optical conductivity of the crystal were calculated for plane polarized light with the polycrystalline approximation. The smearing of 0.2 eV was employed. It is known that DFT calculations tend to underestimate semiconductor band gap values [12], for that reason we have used a 1 eV scissor operator for both crystals.

Calculation of noncovalent interactions

The interaction energies were evaluated at the RI-BP86-D3/def2-TZVP[13-15] level of theory by means of the Turbomole 7.0 program[16] and using the crystallographic coordinates. The basis set superposition error[17] correction scheme was applied to the interaction energies. The QTAIM[18] and NCIPlot[19] analyses were used to characterize the NCIs

using the RI-PB86-D3/def2-TZVP wavefunction and been carried out using the Multiwfn

program[20]and represented using the VMD visualization software[21].

IR and electronic spectra

Distinct bands corresponding to the azomethine (C=N) stretching vibration in the

range of 1637–1645 cm^{-1} are found in the IR spectra of both complexes (Figures S1-S2).[22-23]

Peaks at 2031 and 2098 cm^{-1} indicates the presence of two different types of thiocyanates

(one N-bonded and another one S bonded) in complex **1**.[24] C–H stretching vibrations are

noticed in the range of 2880–2964 cm^{-1}.[25] In complex **1**, bands at 3060 cm^{-1} are assigned as

N–H vibrations.[26]

There are only two bands in the electronic spectra of the complexes (Fig. S3).

Complex **1** shows bands at 267 and 347 nm which may be assigned as $\pi \rightarrow \pi^*$ and LMCT

transitions.[27-28] Complex **2** shows similar bands at 332 and 419 nm respectively. There is no

band corresponding to d–d electronic transitions, in line to our expectation.[29]
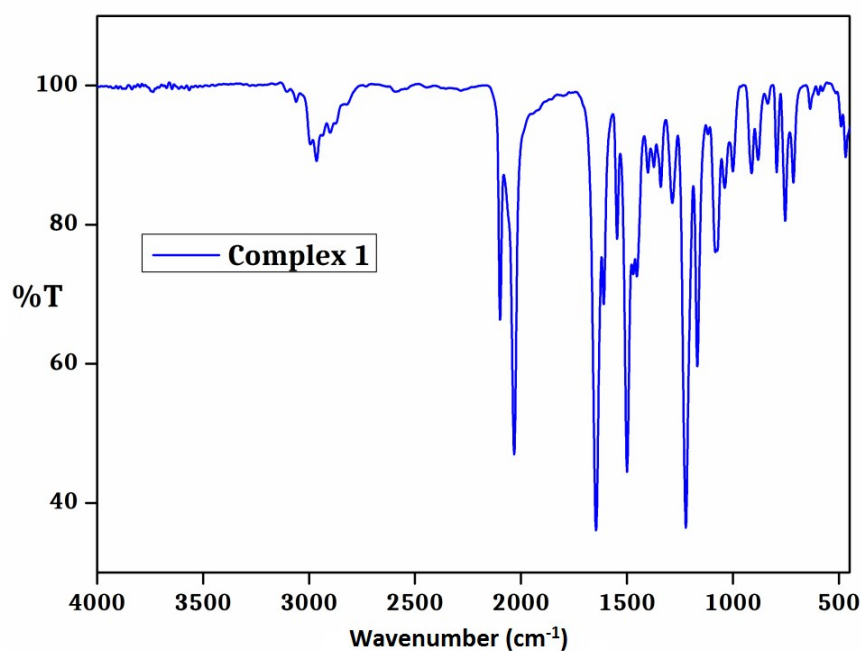
Fig. S1: IR spectrum (KBr pellet) of complex **1.**
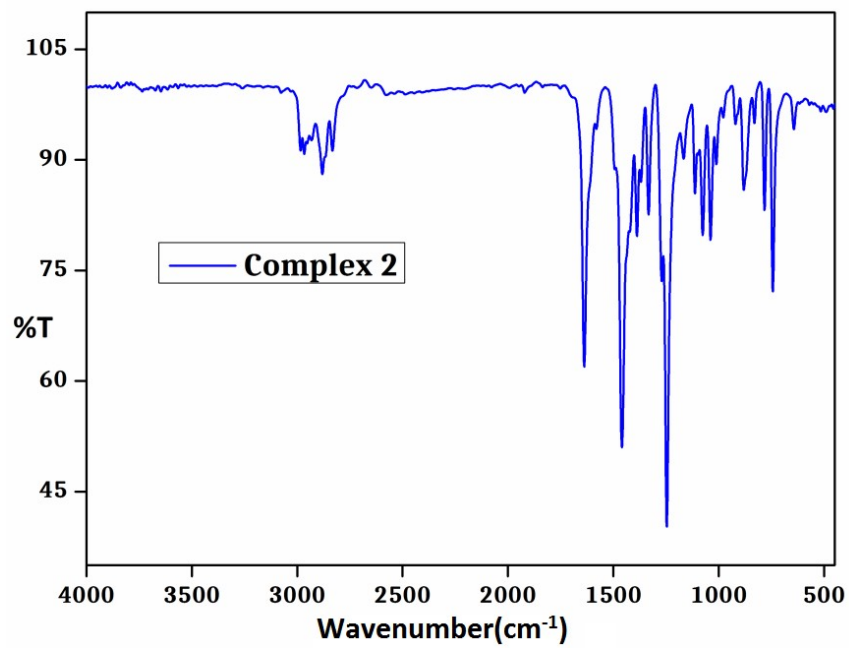
Fig. S2: IR spectrum (KBr pellet) of complex **2.**
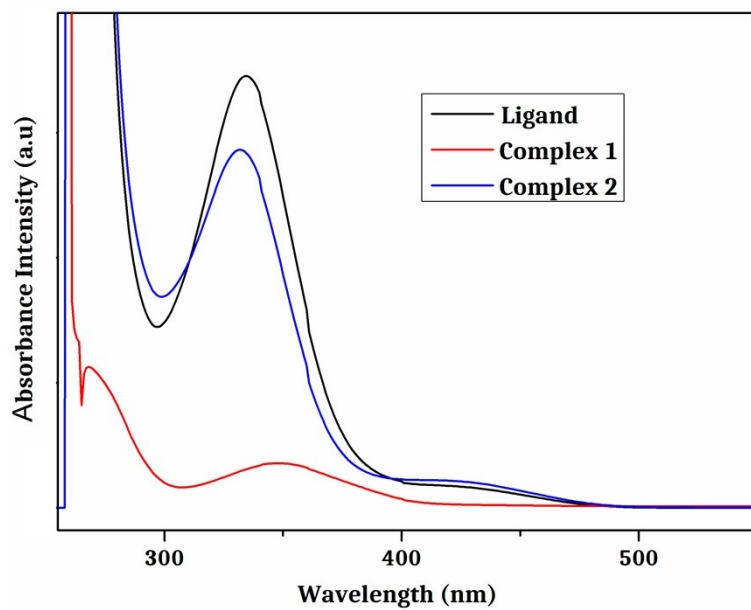
Fig. S3: UV-Vis spectra of ligand and complexes **1,2** in DMF.

Table S1: Crystal data and refinement details of complexes **1** and **2**.

Complex	1	2
Formula	$C_{25}H_{26.64}CdN_4O_4S_2$	$C_{49}H_{63}Cd_3I_2N_5O_9$
Formula Weight	623.67	1457.08
Temperature (K)	293	293
Crystal System	Monoclinic	Triclinic
Space group	$P2_1/n$	$P\text{-}1$
a (Å)	10.4120(13)	11.792(9)
b (Å)	23.504(3)	14.624(12)
c (Å)	11.4415(13)	16.775(13)
α (°)	90	92.589(12)
β (°)	99.147(4)	103.555(9)
γ (°)	90	101.798(10)
Z	4	2
d_{cal} (g cm^{-3})	1.498	1.766
μ(mm^{-1})	0.978	2.335
F(000)	1267	1428
Total reflection	32728	25772
Unique Reflections	5669	12540
Observed data [I>2σ(I)]	3453	7908
R(int)	0.114	0.098
R1, wR2 (all data)	0.1313, 0.1359	0.1338, 0.2515
R1, wR2 [I>2σ(I)]	0.0762, 0.1188	0.0885, 0.2217
CCDC Number	2127905	2127904

Table: S2: Selected bond lengths (Å) of complexes **1** and **2**.

Complex	1	2
Cd(1)–S(2)	2.532(2)	-
Cd(1)–O(3)	2.186(4)	-
Cd(1)–O(4)	2.624(6)	-
Cd(1)–N(3)	2.255(7)	-
Cd(1)–O(1)[a]	2.215(4)	-
Cd(1)–O(2)[a]	2.565(5)	-
Cd(1)–I(1)	-	2.725(3)
Cd(3)–I(2)	-	2.761(3)
Cd(1)–O(1)	-	2.272(9)
Cd(1)–O(2)	-	2.215(9)
Cd(1)–N(1)	-	2.291(10)
Cd(1)–N(2)	-	2.344(10)
Cd(2)–O(1)	-	2.398(9)
Cd(2)–O(2)	-	2.371(9)
Cd(2)–O(3)	-	2.484(9)
Cd(2)–O(4)	-	2.569(9)
Cd(2)–O(5)	-	2.325(9)
Cd(2)–O(6)	-	2.368(8)
Cd(2)–O(7)	-	2.548(8)
Cd(2)–O(8)	-	2.620(9)
Cd(3)–O(5)	-	2.263(8)

Cd(3)–O(6)	-	2.225(9)
Cd(3)–N(3)	-	2.299(11)
Cd(3)–N(4)	-	2.324(9)

Symmetry, a= 1/2-x,-1/2+y,1/2-z.

Table: S3: Selected bond angles (°) of complexes **1** and **2**.

Complex	1	2	Complex	1	2
S(2)-Cd(1)-O(3)	109.83(15)	-	O(1)-Cd(1)-N(2)	-	129.5(3)
S(2)-Cd(1)-O(4)	84.71(13)	-	O(2)-Cd(1)-N(1)	-	133.0(3)
S(2)-Cd(1)-N(3)	109.0(2)	-	O(2)-Cd(1)-N(2)	-	81.8(3)
S(2)-Cd(1)-O(1)a	97.36(13)	-	N(1)-Cd(1)-N(2)	-	83.6(3)
S(2)-Cd(1)-O(2)a	160.58(12)	-	O(1)-Cd(2)-O(2)	-	69.1(3)
O(3)-Cd(1)-O(4)	66.47(16)	-	O(1)-Cd(2)-O(3)	-	64.3(3)
O(3)-Cd(1)-N(3)	92.3(2)	-	O(1)-Cd(2)-O(4)	-	134.5(3)
O(1)a-Cd(1)-O(3)	143.72(17)	-	O(1)-Cd(2)-O(5)	-	141.9(3)
O(2)a-Cd(1)-O(3)	80.78(18)	-	O(1)-Cd(2)-O(6)	-	130.9(3)
O(4)-Cd(1)-N(3)	158.0(2)	-	O(1)-Cd(2)-O(7)	-	85.0(3)
O(1)a-Cd(1)-O(4)	93.59(16)	-	O(1)-Cd(2)-O(8)	-	73.9(3)
O(2)a-Cd(1)-O(4)	84.94(17)	-	O(2)-Cd(2)-O(3)		133.2(3)
O(1)a-Cd(1)-N(3)	101.3(2)	-	O(2)-Cd(2)-O(4)		65.6(3)
O(2)a-Cd(1)-N(3)	86.1(2)	-	O(2)-Cd(2)-O(5)		133.9(3)
O(1)a-Cd(1)-O(2)a	66.97(15)	-	O(2)-Cd(2)-O(6)		119.5(3)
I(1)-Cd(1)-O(1)	-	127.1(2)	O(2)-Cd(2)-O(7)		97.1(3)
I(1)-Cd(1)-O(2)	-	121.4(2)	O(2)-Cd(2)-O(8)		80.4(3)

|				
I(1)-Cd(1)-N(1)	-	105.4(3)	O(3)-Cd(2)-O(4)		161.2(3)
I(1)-Cd(1)-N(2)	-	103.3(3)	O(3)-Cd(2)-O(5)		88.3(3)
O(1)-Cd(1)-O(2)	-	74.1(3)	O(3)-Cd(2)-O(6)		89.6(3)
O(1)-Cd(1)-N(1)	-	81.7(3)	O(3)-Cd(2)-O(7)	-	82.7(3)
O(3)-Cd(2)-O(8)	-	83.5(3)	I(2)-Cd(3)-O(6)	-	120.3(2)
O(4)-Cd(2)-O(5)	-	74.9(3)	I(2)-Cd(3)-N(3)	-	101.7(3)
O(4)-Cd(2)-O(6)	-	76.9(3)	I(2)-Cd(3)-N(4)	-	104.6(2)
O(4)-Cd(2)-O(7)	-	97.4(3)	O(5)-Cd(3)-O(6)	-	74.3(3)
O(4)-Cd(2)-O(8)	-	101.1(2)	O(5)-Cd(3)-N(3)	-	81.5(3)
O(5)-Cd(2)-O(6)	-	70.6(3)	O(5)-Cd(3)-N(4)	-	128.2(3)
O(5)-Cd(2)-O(7)	-	64.6(3)	O(6)-Cd(3)-N(3)	-	138.1(3)
O(5)-Cd(2)-O(8)	-	131.7(3)	O(6)-Cd(3)-N(4)	-	83.0(3)
O(6)-Cd(2)-O(7)	-	134.6(3)	N(3)-Cd(3)-N(4)	-	85.9(4)
O(6)-Cd(2)-O(8)	-	61.8(3)	Cd(1)-O(1)-Cd(2)	-	106.1(3)
O(7)-Cd(2)-O(8)	-	158.2(3)	Cd(2)-O(5)-Cd(3)	-	104.0(3)
I(2)-Cd(3)-O(5)	-	127.2(2)			

Symmetry, ^{a}= 1/2-x,-1/2+y,1/2-z.

PXRD

Experimental PXRD patterns of bulk products are in good agreement with simulated XRD patterns indicating consistency of the bulk sample. Simulated patterns of both complexes have been calculated from the single crystal structural data (Cif files) using Mercury software. The experimental and simulated PXRD patterns of both complexes are shown in Figs. S4 and S5.
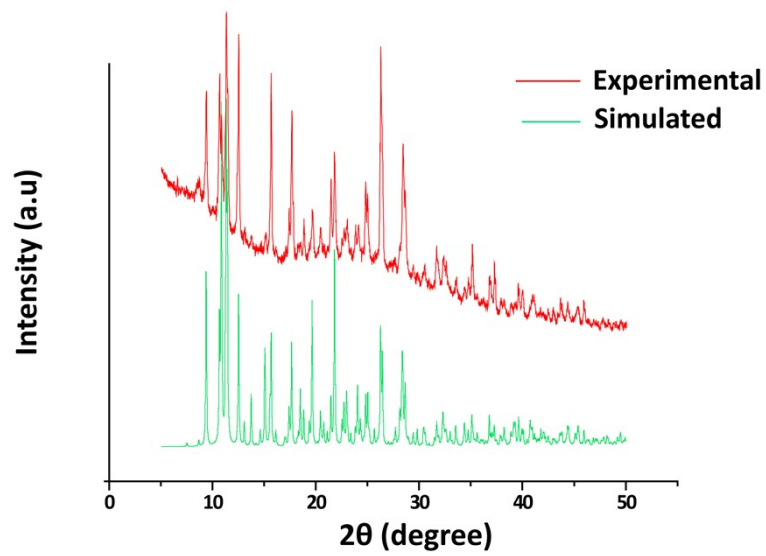
Fig. S4: Experimental and simulated PXRD patterns of complex **1** confirming purity of the
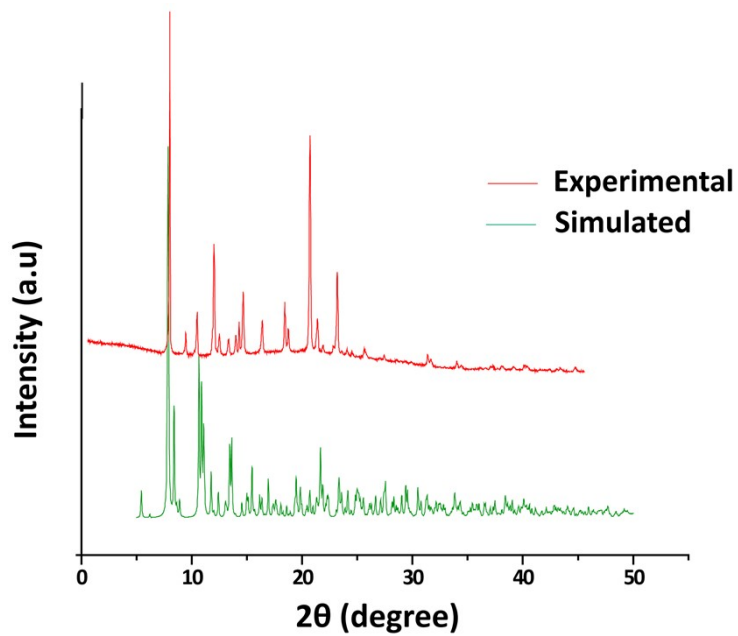
bulk material.

Fig. S5: Experimental and simulated PXRD patterns of complex **2** confirming purity of the

bulk material.

Optical Characterization

The optical band gap (Eg) was calculated using Tauc's equation (Equation S1).[30]

$$\alpha h\nu = A(h\nu - E_g)^n \qquad\qquad \text{(S1)}$$

where α, E_g, h and ν stands for absorption coefficient, band gap, Planck's constant and frequency of light. The exponent 'n' is the electron transition processes dependent constant. 'A' is a constant which is considered as 1 for ideal case. To calculate the direct optical band gap the value of the exponent 'n' in the above equation has been considered as $n = ½$.[30] By extrapolating the linear region of the plot $(\alpha h\nu)^2$ *vs. hv* (Fig. 6) to $\alpha = 0$ absorption, the values of optical direct band gap (E_g) have been calculated as 3.58 eV, 3.21 eV and 3.43 eV for synthesized ligand and complexes **1** and **2** respectively.

Device Fabrication

In this study, multiple metal-semiconductor (MS) junction devices were fabricated in ITO/synthesized complex/Al sandwich structure to perform the electrical study. In this regard, well dispersion of the synthesized complexes were made in N,N-dimethyl formamide (DMF) by mixing and sonicated the right proportion (25 mg/ml) of the complex in separate vials. This freshly prepared stable dispersion of the complexes was deposited on the top of the ITO coated glass substrate by spun firstly at 600 rpm for 5 min and thereafter at 900 rpm for another 5 min with the help of SCU 2700 spin coating unit. Afterward, the as-deposited thin films were dried in a vacuum oven at 80 °C for several minutes to evaporate the solvent part fully. Here we used aluminium as metal electrode, which was deposited using Vacuum Coating Unit on the active layer of the devices by maintaining the effective area as 7.065×10^{-2} cm^{-2} with shadow mask. Using Sourcemeter made by Keithley (model no: 2635B), the current-voltage (I-V) characteristics of the devices was measured to analyze

the electrical properties. All the device fabrication and measurements were carried out at room temperature and under ambient conditions.

Electrical Characterization

The *I–V* characteristic of **CD1** and **CD2** was further analyzed by thermionic emission theory. Cheung's method was also been employed to extract important diode parameters.[30] In this regard, the obtained *I–V* curve was analyzed quantitatively by considering the following standard equations:[30,31]

$$I = I_0 exp\left(\frac{qV}{\eta KT}\right)\left[1 - exp\left(\frac{-qV}{\eta kT}\right)\right] \quad \text{(S2)}$$

$$I_0 = AA^*T^2 exp\left(\frac{-q\emptyset_B}{kT}\right) \quad \text{(S3)}$$

where, I_0, k, T, V, A, η and A^* stands for saturation current, electronic charge, Boltzmann constant, temperature in Kelvin, forward bias voltage, effective diode area, ideality factor and effective Richardson constant, respectively. The effective diode area has been estimated as 7.065×10^{-2} cm^2 and the effective Richardson constant has been considered as 32 AK^{-2} cm^{-2} for all the devices.

The series resistance, ideality factor and barrier potential height was also determined by using equations S4 to S6, which was extracted from Cheung's idea,[32,33]

$$\frac{dV}{dln(I)} = \left(\frac{\eta kT}{q}\right) + IR_S \quad \text{(S4)}$$

$$H(I) = V - \left(\frac{\eta kT}{q}\right)\ln\left(\frac{I_S}{AA^*T^2}\right) \quad \text{(S5)}$$

$$H(I) = IR_S + \eta\emptyset_B \quad \text{(S6)}$$

From the saturated values of capacitance at the higher frequency regime (Fig. S6) the dielectric permittivity of the complex was calculated using following equation[30]:

$$\varepsilon_r = \frac{1}{\epsilon_0}.\frac{C.D}{A}$$

(S7)

where, C is the capacitance (at saturation), D is the thickness of the film which has been considered as ~1 µm and A is the effective area. Using the above formula, the relative dielectric constant of the material has been estimated as 4.87×10^{-2} and 6.63×10^{-2} for complexes **1** and **2** respectively.
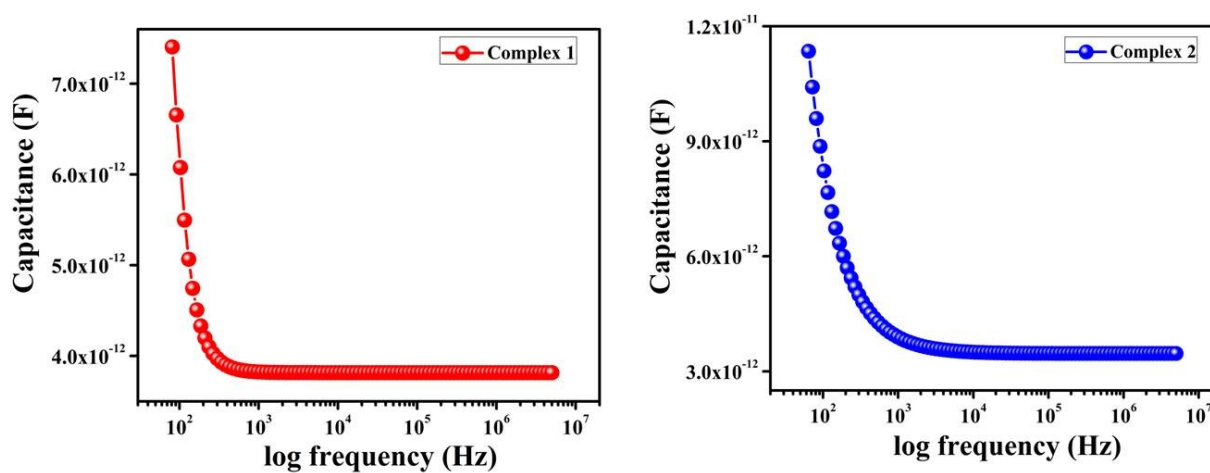
Fig. S6: Capacitance vs. Frequency graph of complexes **1** and **2**.

Ligand DFT study

The ligand was modelled using DFT calculations and using as starting point for the optimization the X-ray coordinates. The standard band theory was used to calculate the band gap and the DOS. Fig. S7 shows the band diagram of the ligand that is quite different compared to the metal complexes, which present a flatter conduction band. The calculated band gap is 3.73 eV, which is in reasonable agreement with the experimental value (3.58 eV, see Fig. 6, main text). These calculations correspond to the convergent mode of the ligand. In case of using the divergent mode for the calculation of the ligand, the computed band gap is only 2.83 eV, showing a much worst agreement with the experimental value.
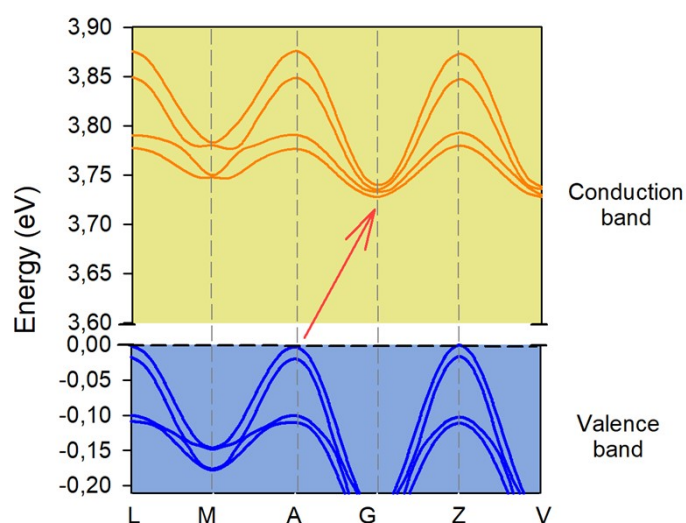
Fig. S7: Electronic band structures of the ground state of the ligand. Points of high symmetry in the first Brillouin zone are labelled as follows: Left Panel) Z = (0, 0, 0.5); G = (0, 0, 0); Y = (0, 0.5, 0); A = (-0.5, 0.5, 0); B = (-0.5, 0, 0); D = (-0,5, 0, 0.5); E = (-0.5, 0.5, 0.5); C = (0, 0.5, 0.5). Center Panel) G = (0, 0, 0); F = (0, 0.5, 0); Q = (0, 0.5, 0.5); Z = (0, 0, 0.5). Right Panel) L = (-0.5, 0, 0.5); M = (-0.5, 0.5, 0.5); A = (-0.5, 0, 0); G = (0, 0, 0); Z =(0, -0.5, 0.5); V = (0, 0, 0.5). The red arrow marks the band gap.

Fig. S8 shows the partial density of states analysis of the ligand. It is revealed that both valence and conduction bands are mainly dominated by the p-orbitals, in line with the aromatic character of the ligand.
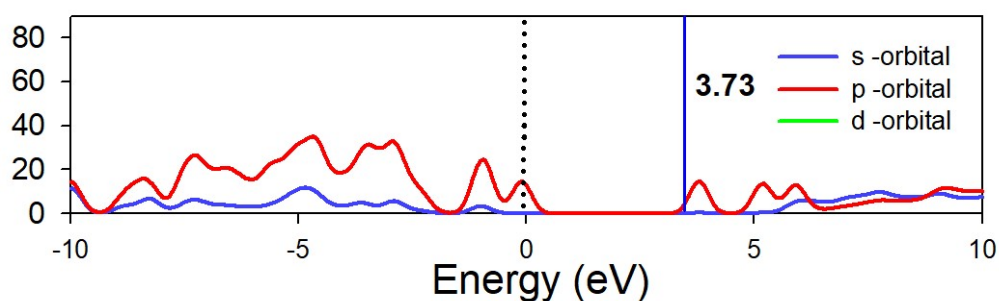
Fig. S8: Calculated total and partial density of states of the ligand. The lines represent the s-orbital character (blue), p-orbital character (red) and d-orbital character /green) of the atoms into the crystal.

Table S4: Conductivity parameters for reported metal-ligand complexes (polymers) in CCDC.

CCDC code & Complex Formula	Conductivity [S.m^{-1}] (Condition)	Reference	CCDC code & Complex Formula	Conductivity [S.m^{-1}] (Condition)	Reference
PUMCIL [Cd(3-bpd)(SCN)$_2$]$_n$	4.53×10^{-5} (Dark) 1.93×10^{-4} (Light)	34	**XADPAX** [Cu(nip)(4-phpy)$_2$]$_n$	7.56×10^{-6} (Dark)	39
EHENEN [Pb$_2$(bdc)$_{1.5}$(aiz)]$_n$	2.94×10^{-6} (Dark) 6.12×10^{-6} (Light)	35	**CURQIR** [CdL^1(μ-$_{1,3}$-SCN)$_2$]$_n$	1.01×10^{-6} (Dark) 2.16×10^{-6} (Light)	40
EHENIR [Pb$_2$(bdc)$_{1.5}$(aiz)(MeOH)$_2$]$_n$	2.92×10^{-7} (Dark) 3.66×10^{-7} (Light)		**QESXOE** [Cu$_2$L$^2{}_2$(μ-$_{1,3}$-SCN)$_2$]$_n$	3.63×10^{-5} (Dark) 4.13×10^{-5} (Light)	41
SAHXEH [Cd(adc)(4-phpy)$_2$(H$_2$O)$_2$]	1.53×10^{-5} (Dark) 3.04×10^{-5} (Light)	36	**ZIJTOE** [{CuL^{3}Na}$_2$(μ-$_{1,1,3}$-NCS)HgCl(μ-Cl)(μ-$_{1,3}$-NCS)]$_n$	1.48×10^{-6} (Dark) 8.40×10^{-6} (Light)	42
SAHXIL [Zn(adc)(4-phpy)$_2$(H$_2$O)$_2$]	5.9×10^{-6} (Dark) 7.78×10^{-6} (Light)		**VINWUN** [(NCS)Pb(H$_2$O)L^{3}Ni(NCS)]$_n$	6.02×10^{-4} (Dark) 3.47×10^{-3} (Light)	43
CIDGOO [Cu$_2$(muco)$_2$(py)$_4$]·4H$_2$O·2EtOH	7.54×10^{-5} (Dark) 1.99×10^{-4} (Light)	37	**FOZXOK** {[Cd(suc)(4-nvp)$_2$]·2H$_2$O}$_n$	1.18×10^{-3} (Dark) 1.68×10^{-3} (Light)	44
RAJDEP	7.51×10^{-4}	38	**TOVJOG**	0.88×10^{-8}	45

Name/Formula	Value	Ref	Name/Formula	Value	Ref
[{Cd$_2$(cis-1,4-chdc)$_2$(1,10-phen)$_2$}·5H$_2$O]$_n$	(Dark)		[(N$_3$)CoL^{4}Na(N$_3$)]$_n$	(Dark) 2.38×10^{-8} (Light)	
INUKIL [Zn$_2$(phen)$_2$(e,a-cis-1,4-chdc)2(H$_2$O)$_2$]$_n$	2.52×10^{-4} (Dark)		**TECNUN** [Cd(4-bpd)(SCN)$_2$]$_n$	2.90×10^{-4} (Dark) 7.16×10^{-4} (Light)	46
RUKXUT [Co(adc)(4-ppy)(H$_2$O)$_2$]$_n$	2.61×10^{-5} (Dark)	47	**XOZSEN** [Zn(*cis*-1,4-chdc)(py)]$_n$	1.09×10^{-3} (Dark)	53
RUKYAA [Co(adc)(4-bppy)(H$_2$O)$_2$]$_n$	2.52×10^{-6} (Dark)		**XOZSIR** [Zn(*cis*-1,4-chdc)(4-phpy)]$_n$	6.01×10^{-5} (Dark)	
VAXVOJ [Zn$_4$(bdc)$_4$(ppmh)$_2$(H$_2$O)$_n$	1.37×10^{-6} (Dark)	48	**DEHPUE** [Cd$_4$L^5$_2$(NCO)$_6$]$_n$	2.90×10^{-4} (Dark) 7.16×10^{-4} (Light)	54
XOSFOD [Cu$_2$(DABA)$_4$(4,4'-BPY)]$_n$	2.65×10^{-6} (Dark)	49	**MAWPOS** [Zn(INH)(succ)]$_n$	2.26×10^{-4} (Dark)	55
XOSFUJ [Cu$_4$(DABA)$_8$(PYZ)(H$_2$O)$_2$]	3.12×10^{-4} (Dark)		**MAWPUY** [Zn(INH)(bdc)]$_n$	1.12×10^{-4} (Dark)	
TOHVIY [Cd(bpe)(*p*-brba)$_2$]$_n$	1.05×10^{-3} (Dark)	50	**MAWQEJ** [Zn(INH)(fum)]$_n$	1.25×10^{-4} (Dark)	
TOHVOE [Cd(*rctt*-tpcb)$_{1/2}$(*p*-brba)$_2$]$_n$	1.85×10^{-6} (Dark)		**CIJLEP** [Cd(2,2'-dsb)(4-nvp)(DMF)(H$_2$O)]	6.60×10^{-4} (Dark) 10.71×10^{-4} (Light)	56
ASEXEE [Zn(adc)(4-nvp)$_2$(H$_2$O)$_2$]$_n$	9.29×10^{-4} (Dark) 16.58×10^{-4}	51	**CEZMUS** Cd(adc)(4-nvp)$_2$(H$_2$O)]$_n$	1.83×10^{-3} (Dark)	57

	(Light)				
MIFSIG {[Zn(adc)(4-spy)$_2$(H$_2$O)$_2$]}$_n$	5.12×10^{-4} (Dark) 16.48×10^{-4} (Light)	52	**VINZUQ** [Cu(ptha)$_2$(pyraz)(H$_2$O)$_2$]$_n$	2.34×10^{-6} (Dark) 7.60×10^{-6} (Light)	59
FEXVAI {[Cd(adc)(4-spy)$_2$(H$_2$O)$_2$]}$_n$	6.54×10^{-4} (Dark) 28.77×10^{-4} (Light)		**GOBFOV** {[Cd$_2$(anc)$_2$(4-nvp)$_6$]·(MeOH)·(H$_2$O)}$_n$	6.91×10^{-4} (Dark) 13.90×10^{-4} (Light)	60
YOTTUZ [Cd(HL^6$_2$)$_2$(N(CN)$_2$)$_2$]$_n$	1.26×10^{-6} (Dark) 6.72×10^{-5} (Light)		**Complex 1 (CD1)**	3.89×10^{-4} (Dark) 8.25×10^{-4} (Light)	**This work**
YOTVAH Cd$_2$(L^7)$_2$(NCS)$_2$(CH$_3$OH)	1.78×10^{-7} (Dark) 6.15×10^{-7} (Light)	58	-	-	-
YOTVEL [Cd(HL^7)$_2$(N(CN)$_2$)$_2$.H$_2$O]$_n$	1.07×10^{-7} (Dark) 2.44×10^{-7} (Light)		-	-	-

3-bpd = 1,4-bis(3-pyridyl)-2,3-diaza-1,3-butadiene; aiz = (E)-N'-(thiophen-2-ylmethylene)isonicotinohydrazide); H$_2$adc = acetylenedicarboxylic acid and 4-phpy = 4-phenylpyridine; H$_2$muco = trans-muconic acid, py = pyridine; 1,4-H$_2$chdc = 1,4-cyclohexanedicarboxylic acid, 1,10-phen = 1,10-phenanthroline; chdc = cyclohexanedicarboxylic acid; H$_2$nip = 5-nitroisophthalic acid and 4-phpy = 4-phenylpyridine; HL^1 = 2-(2-(ethylamino)ethyliminomethyl)-6-ethoxyphenol; HL^2 = 2-(2-(ethylamino)ethylimino)methyl)-6-ethoxyphenol; H$_2$L^3 = N,N'-bis(3-methoxysalicylidene)propane-1,3-diamine}; H$_2$suc = succinic acid and 4-nvp = 4-(1-naphthylvinyl)pyridine); H$_2$L^4 = [N,N'-bis(5-bromo-3-methoxysalicylidene)-2,2-dimethylpropane-1,3-diamine]; 4-bpd = 1,4-bis(4-pyridyl)-2,3-diaza-1,3-butadiene; 4-ppy = 4-phenylpyridine; 4-bppy = 4-(4-bromophenyl)pyridine); H$_2$bdc = 1,4-benzene dicarboxylic acid, ppmh = N-pyridin-2-yl-N'-pyridin-4-ylmethylene-hydrazine; 4,4'-BPY = 4,4'-bipyridine,

PYZ = pyrazine, HDABA = 4-diallylamino-benzoic acid; bpe = 1,2-bis(4-pyridyl)ethylene, *p*-brba = *para*-bromobenzoic acid; *rctt*-tpcb = *rctt*-tetrakis(4-pyridyl)cyclobutane; 4-nvp = 4-(1-naphthylvinyl)pyridine; 4-spy = 4-styrylpyridine; HL[5] = (E)-2-methoxy-6- ((quinolin-8-ylimino)methyl)phenol; INH = isoniazid, H_2succ = succinic acid, H_2fum = fumaric acid, H_2bdc = terephthalic acid; $H_2$2,2'-dsb = 2,2'-disulfanediyldibenzoic acid, 4-nvp = 4-(1-naphthylvinyl)pyridine; HL[6]= (E)-2-methoxy-6-((quinolin-5-ylimino)methyl)phenol; HL[7] = (E)-2-methoxy-6-{(quinolin-3-ylimino)methyl}phenol, H_2ptha = phthalic acid, pyraz = pyrazine; H_2anc = 9,10-anthracenedicarboxylic acid.

Table S5: Conductivity parameters for reported metal-ligand complexes (not polymer) in CCDC.

CCDC code Complex Formula	Conductivity (S.m^{-1})	Reference
AKIVIC $[(N_3)Co^{III}L^8(\mu-C_6H_4(NO_2)CO_2)Co^{II}(N_3)]$	2.04×10^{-5} (Dark)	61
AKIVOI $[(N_3)Co^{III}L^9(\mu-C_6H_4(NO_2)CO_2)Co^{II}(N_3)]$	2.58×10^{-4} (Dark)	
QUXHOJ $[Cd_4L^{10}_2(NO_3)_2(\mu_{1,1}-N_3)_2(CH_3OH)_2]$	13.1×10^{-8}(Dark) 11.2×10^{-7}(Light)	62
QUXHUP $\{[Cd_2L^{10}(IPA)]_2 \cdot (CH_3OH)\}_n$	5.4×10^{-8} (Dark) 13.5×10^{-7} (Light)	
GEYYIV $[Cu_2(adc)(4-pic)_6(H_2O)_4][ClO_4]_2$	8.21×10^{-4} (Dark) 11.84×10^{-4} (Light)	63
SUVVEN $[CuL^{11}(NCS)]$	6.49×10^{-4} (Dark) 21.29×10^{-4} (Light)	64
NITBEA	7.47×10^{-4} (Dark)	65

[(NCS)(H$_2$O)NiL^{4}Pb(DMF)Cl]$_2$	23.12 × 10^{-4} (Light)	
JUCLUR [(N$_3$)$_2$CoL^{12}Na(DMF)]	1.01 × 10^{-5} (Dark) 2.56 × 10^{-5} (Light)	66
TUTROS [Fe(L^{13})(N$_3$)]	16.3 × 10^{-5} (Dark)	67
TUTCET [Fe(L^{14})(N$_3$)]	1.02 × 10^{-5} (Dark)	
VINQUH [Cu$_2$(ptha)$_4$(2-ampy)·(H$_2$O)]	2.02 × 10^{-6} (Dark) 4.34 × 10^{-6} (Light)	59
Complex 2 (CD2)	1.81 × 10^{-4} (Dark) 4.72 × 10^{-4} (Light)	**This work**

H$_2$L^8 = (2,2-dimethyl-1,3-propanediyl)bis(iminomethylene)bis(6-methoxyphenol), H$_2$L^9 = (2,2-dimethyl-1,3-propanediyl)bis(iminomethylene)bis(6-ethoxyphenol)}; H$_2$L^{10} = (*N,N'*-bis(3-methoxysalicylidene)-diethylenetriamine); IPA = isophthalic acid; H$_2$adc = acetylenedicarboxylic acid, 4-pic = 4-picolene; HL^{11} = (1-(2-(diethylamino)ethylimino)ethyl)naphthalene-2-ol; H$_2$L^{12} = [N,N'-bis(3-ethoxysalicylidene)-2,2-dimethylpropane-1,3-diamine]; H$_2$L^{13} = *N,N'*-bis(3-methoxysalicylidene)diethylenetriamine, H$_2$L^{14} = *N,N'*-bis(3-ethoxysalicylidene)diethylenetriamine; 2-ampy = 2-aminopyrimidine.

References

(1) G. M. Sheldrick, SADABSs: An Empirical Absorption Correction Program, Bruker Analytica X-ray Systems: Madison, WI, 1996.

(2) L. J. Farrugia, J. *Appl. Cryst.*, 2012, **45**, 849–854.

(3) G. M. Sheldrick, *Acta Crystallogr. Sect. A*, 2008, **64**, 112–122.

(4) G. M. Sheldrick, *Acta Crystallogr. Sect. C*, 2015, **71**, 3–8.

(5) C. F. Macrae, I. J. Bruno, J. A. Chisholm, P. R. Edgington, P. McCabe, E. Pidcock, L. R. Monge, R. Taylor, J van de Streek and P. A. Wood, *J. Appl. Crystallogr.*, 2008, **41**, 466–470.

(6) S. J. Clark, M. D. Segall, C. J. Pickard, P. J. Hasnip, M. I. J. Probert, K. Refson and M. C. Payne, *Z. Kristallogr.*, 2005, **220**, 567–570.

(7) J. P. Perdew, K. Burke and M. Ernzerhof, *Phys. Rev. Lett.*, 1996, **77**, 3865–3868.

(8) J. P. Perdew, J. A. Chevary, S. H. Vosko, K. A. Jackson, M. R. Pederson, D. J. Singh and C. Fiolhais, *Phys. Rev. B.*, 1992, **46**, 6671–6687.

(9) D. Vanderbilt, *Phys. Rev. B* **1990**, *41*, 7892-7895.

(10) D. D. Koelling and B. N. Harmon, *J. Phys. C: Solid State Phys.*, 1977, **10**, 3107–3114.

(11) S. Grimme, *J. Comput. Chem.*, 2006, **27**, 1787-1799.

(12) J. P. Perdew and M. Levy, *Phys. Rev. Lett.*, 1983, **51**, 1884-1887.

(13) C. Adamo and V. Barone, *J. Chem. Phys.*, 1999, **110**, 6158–6170.

(14) F. Weigend, *Phys. Chem. Chem. Phys.*, 2006, **8**, 1057-1065.

(15) S. Grimme, J. Antony, S. Ehrlich and H. Krieg, *J. Chem. Phys.*, 2010, **132**, 154104.

(16) R. Ahlrichs, M. Bär, M. Hacer, H. Horn and C. Kömel, *Chem. Phys. Lett.*, 1989, **162**, 165-169.

(17) S. F.; Boys and F. Bernardi, *Mol. Phys.*, 1970, **19**, 553-566.

(18) R. F. W. Bader, *Chem. Rev*., 1991, **91**, 893–928.

(19) J. Contreras-Garcia, E. R. Johnson, S. Keinan, R. Chaudret, J. P. Piquemal, D. N. Beratan and W. Yang, *J. Chem. Theory Comput*., 2011, **7**, 625-632.

(20) T. Lu and F. Chen, *J. Comput. Chem*., 2012, **33**, 580–592.

(21) J. W. Humphrey, A. Dalke and K. Schulten, *J. Mol. Graph*., 1996, **14**, 33–38.

(22) P. Bhowmik, H. P. Nayek, M. Corbella, N. Aliaga-Alcalde and S. Chattopadhyay, *Dalton Trans*., 2011, **40**, 7916-7926.

(23) S. Roy, D. Sutradhar, M. G. B. Drew and S. Chattopadhyay, *CrystEngComm,* 2021, **23**, 6724-6735.

(24) S. Roy, A. Bhattacharyya, S. Purkait, A. Bauzá, A. Frontera and S. Chattopadhyay, *Dalton Trans*., 2016, **45**, 15048-15059.

(25) S. Roy, M. G. B. Drew and S. Chattopadhyay, *Polyhedron,* 2018, **150**, 28-34.

(26) A. Banerjee, A. Frontera and S. Chattopadhyay, *Inorg. Chim. Acta,* 2021, **521**, 120298-120306.

(27) M. Karmakar, S. Roy and S. Chattopadhyay, *New J. Chem*., 2019, **43**, 10093-10102.

(28) K. Ghosh, K. Harms and S. Chattopadhyay, *Polyhedron*, 2017, **123**, 162–175.

(29) S. Roy, I. Mondal, K. Harms and S. Chattopadhyay, *Polyhedron,* 2019, **159**, 265-274.

(30) A. Dey, S. Middya, R. Jana, M. Das, J. Datta, A. Layek and P. P. Ray, *J. Mater. Sci.: Mater. Electron*., 2016, **27**, 6325-6335.

(31) E. H. Rhoderick, Metal Semiconductors Contacts, Oxford University Press, Oxford. 1978.

(32) S. K. Cheung and N. W. Cheung, *Appl. Phys. Lett*., 1986, **49**, 85-87.

(33) A. Dey, A. Layek, A. Roychowdhury, M. Das, J. Datta, S. Middya, D. Das and P. P. Ray, *RSC Adv.,* 2015, **5**, 36560-36567.

(34) S. Halder, A. Layek, K. Ghosh, C. Rizzoli, P. P. Ray and P. Roy, *Dalton Trans*., 2015, **44**, 16149-16155**.**

(35) S. Dey, S. Sil, B. Dutta, K. Naskar, S. Maity, P. P. Ray and C. Sinha, *ACS Omega,* 2019, **4**, 19959–19968.

(36) F. Ahmed, J. Ortega-Castro, A. Frontera and M. H. Mir, *Dalton Trans*., 2021, **50**, 270–278.

(37) F. Ahmed, J. Datta, S. Sarkar, B. Dutta, A. D. Jana, P. P. Ray and M. H. Mir, *ChemistrySelect,* 2018*,* **3***,* 6985-6991**.**

(38) Akhtaruzzaman, B. Pal, S. Khan, B. Dutta, S. Naaz, S. Maity, P. Ghosh, P. P. Ray and M. H. Mir, *CrystEngComm,* 2021, **23**, 7525-7533**.**

(39) S. Islam, P. Das, S. Maiti, S. Khan, S. Maity, P. Ghosh, A. D. Jana, P. P. Ray and M. H. Mir, *Dalton Trans*., 2020, **49**, 15323-15331.

(40) S. Roy, A. Dey, P. P. Ray, J. Ortega-Castro, A. Frontera and S. Chattopadhyay, *Chem. Commun*., 2015, **51**, 12974-12976.

(41) S. Khan, S. Halder, P. P. Ray, S. Herrero, R. Gonzalez-Prieto, M. G. B. Drew and S. Chattopadhyay, *Cryst. Growth Des*., 2018, **18**, 651–659.

(42) S. Roy, S. Halder, M. G. B. Drew, P. P. Ray and S. Chattopadhyay, *New J. Chem*., 2018, **42**, 15295-15305.

(43) S. Roy, S. Halder, M. G. B. Drew, P. P. Ray and S. Chattopadhyay, *ACS Omega,* 2018, **3**, 12788−12796.

(44) B. Dutta, A. Hazra, A. Dey, C. Sinha, P. P. Ray, P. Banerjee and M. H. Mir, *Cryst. Growth Des*., 2020, **20**, 765−776.

(45) K. Ghosh, S. Sil, P. P. Ray, J. Ortega-Castro, A. Frontera and S. Chattopadhyay, *RSC Adv*., 2019, **9**, 34710-34719.

(46) S. Halder, A. Dey, A. Bhattacharjee, J. Ortega-Castro, A. Frontera, P. P. Ray and P. Roy, *Dalton Trans*., 2017, **46**, 11239-11249.

(47) F. Ahmed, J. Datta, S. Khan, B. Dutta, S. Islam, S. Naaz, P. P. Ray and M. H. Mir, *New J. Chem*., 2020, **44**, 9004-9009.

(48) A. Chandra, M. Das, K. Pal, S. Jana, B. Dutta, P. P. Ray, K. Jana and C. Sinha, *ACS Omega,* 2019, **4**, 17649−17661.

(49) S. Jana, R. Jana, S. Sil, B. Dutta, H. Sato, P. P. Ray, A. Datta, T. Akitsu and C. Sinha, *Cryst. Growth Des*., 2019, **19**, 6283−6290.

(50) S. Islam, J. Datta, S. Maity, B. Dutta, S. Khan, P. Ghosh, P. P. Ray and M. H**.** Mir, *Cryst. Growth Des*., 2019, **19**, 4057−4062.

(51) B. Dutta, A. Dey, S. Maity, C. Sinha, P. P. Ray and M. H. Mir, *ACS Omega,* 2018, **3**, 12060−12067.

(52) B. Dutta, A. Dey, K. Naskar, S. Maity, F. Ahmed, S. Islam, C. Sinha, P. Ghosh, P. P. Ray and M. H. Mir, *New J. Chem*., 2018, **42**, 10309-10316.

(53) Akhtaruzzaman, P. Das, S. Khan, S. Maity, S. Naaz, S. Islam, P. Ghosh, P. P. Ray and M. H. Mir, *New J. Chem*., 2019, **43**, 16071-16077.

(54) P. Ghorai, A. Dey, P. Brandao, J. Ortega-Castro, A. Bauza, A. Frontera, P. P. Ray and A. Saha, *Dalton Trans*., 2017, **46**, 13531-13543.

(55) K. Naskar, A. Dey, B. Dutta, F. Ahmed, C. Sen, M. H. Mir, P. P. Ray and C. Sinha, *Cryst. Growth Des*., 2017, **17**, 3267–3276.

(56) B. Dutta, R. Jana, C. Sinha, P. P. Ray and M. H. Mir, *Inorg. Chem. Front*., 2018, **5**, 1998-2005.

(57) B. Dutta, A. Dey, C. Sinha, P. P. Ray and M. H. Mir, *Inorg. Chem*., 2018, **57**, 8029–8032.

(58) P. Ghorai, A. Dey, A. Hazra, B. Dutta, P. Brandao, P. P. Ray, P. Banerjee and A. Saha, *Cryst. Growth Des*., 2019, **19**, 6431–6447.

(59) A. Hossain, A. Dey, S. K. Seth, P. P. Ray, P. Ballester, R. G. Pritchard, J. Ortega-Castro, A. Frontera and S. Mukhopadhyay, *ACS Omega,* 2018, **3**, 9160–9171.

(60) B. Dutta, R. Jana, A. K. Bhanja, P. P. Ray, C. Sinha and M. H. Mir, *Inorg. Chem*., 2019, **58**, 2686–2694.

(61) A. Banerjee, D. Das, P. P. Ray, S. Banerjee and S. Chattopadhyay, *Dalton Trans.,* 2021, **50**, 1721–1732.

(62) T. K. Ghosh, S. Jana, S. Jana and A. Ghosh, *New J. Chem*., 2020, **44**, 14733-14743.

(63) B. Dutta, A. Dey, K. Naskar, F. Ahmed, R. Purkait, S. Islam, S. Ghosh, C. Sinha, P. P. Ray and M. H. Mir, *New J. Chem*., 2018, **42**, 8629-8637.

(64) S. Khan, S. Halder, A. Dey, B. Dutta, P. P. Ray and S. Chattopadhyay, *New J. Chem*., 2020, **44**, 11622-11630.

(65) S. Roy, A. Dey, M. G. B. Drew, P. P. Ray and S. Chattopadhyay, *New J. Chem*., 2019, **43**, 5020-5031.

(66) S. Roy, S. Halder, A. Dey, K. Harms, P. P. Ray and S. Chattopadhyay, *New J. Chem*., 2020, **44**, 1285-1293.

(67) T. Basak, D. Das, P. P. Ray, S. Banerjee and S. Chattopadhyay, *CrystEngComm,* 2020, **22**, 5170–5181.